Journal of Marine Science and Application (2026) 25: 561-574
https://doi.org/10.1007/s11804-025-00626-3

RESEARCH ARTICLE

Mutual Influence of Welding Residual Stress Redistribution and Surface Crack Propagation

Haiyang Gao[1], Guangen Luo[1], Pengfei Xu[1], Ying Chai[1] and Liangbi Li[1]

Received: 01 February 2025 / Accepted: 04 March 2025

Abstract

The crack propagation life of welded ship structures is considerably influenced by welding residual stresses, which are redistributed as cracks propagate. Therefore, studying the mutual interaction between welding residual stress redistribution and surface crack propagation is crucial for accurately predicting the crack propagation life of welded structures. This research uses TC4 titanium alloy specimens, applying the extended finite element method to investigate the welding residual stress redistribution during surface crack propagation. The cyclic iteration analysis method is proposed to simultaneously consider the redistribution of welding residual stresses and crack propagation. The results show that 1) the welding residual stresses at the surface crack tip and crack depth initially increase, then decrease with crack propagation, and 2) the predicted fatigue crack propagation life, when welding residual stress is not considered, is 2.01 times longer than the corresponding fatigue crack propagation life using the proposed method, which accounts for welding residual stress. In addition, when the welding residual stress is set to a constant value of 0.3 σ_y, the fatigue crack propagation life prediction becomes overly conservative, yielding only 0.39 times the fatigue crack propagation life predicted based on the mutual influence of welding residual stress redistribution. The fatigue crack propagation life prediction method proposed in this study, which considers the interaction between welding residual stress redistribution and crack propagation, offers a more reasonable approach. It lays the foundation for accurate prediction of fatigue crack propagation life in welded structures.

Keywords Fatigue crack propagation; Welding residual stress redistribution; Extended finite element method; Mutual influence analysis; Surface crack

1 Introduction

Welding residual stress, which is produced during ship structure fabrication, is generally detrimental to the structure's safety. The fatigue life assessment of ship structures can be influenced by the welding residual stress field, affecting the structure's mean and peak cyclic stresses (Zhang et al., 2018). Previous studies often approximated welding residual stress as a constant value to assess its impact on fatigue life (Hou W, 1990). However, under fatigue loading, the welding residual stress continually evolves. Initially, under high-level cyclical loading, the combined stress from cyclical loading and welding residual stress at the fatigue hot spot may surpass the yield stress, thereby releasing welding residual stress. Furthermore, welding residual stress is internally balanced within a structure, compromising the load-bearing capacity of the new crack surface area as the crack propagates. Consequently, the welding residual stress near the crack is continually redistributed. These types of welding residual stress redistributions may influence crack propagation.

In recent years, the release of welding residual stress under fatigue loading has been investigated. Li and Wang (2009) summarized the relationship between the magnitude of fatigue loading and the degree of welding residual stress release. They explored the mechanism of welding residual stress release, emphasizing that when external loads are combined with residual stress, causing the fatigue hot spot

Article Highlights

- An analysis method for predicting the surface crack propagation life of ship welded joints is proposed using the extended finite element method and an extended McEvily model. This approach considers the interactions between crack propagation and welding residual stress.
- This study found that the welding residual stress at the crack tip was gradually released during crack propagation, whereas the welding residual stress ahead of the crack tip was dynamically redistributed with crack propagation.
- The proposed method can track the welding residual stress redistribution and release ahead of the crack tip, whereas the redistributed residual stress affects further crack propagation.
- This method can predict the fatigue crack propagation life of ship welded structures more accurately than the traditional methods.

✉ Guangen Luo
luoge@just.edu.cn

[1] School of Naval architecture and Ocean Engineering, Jiangsu University of Science and Technology, Zhenjiang 212100, China

stress to exceed the material's yield stress, the structural material enters the plastic stage, releasing the residual stress within the structure. Zaroog et al. (2011) established an empirical model to estimate compressive residual stress relaxation. The initial compressive residual stresses are released during component operating life. Xie et al. (2017) proposed an analytical model that accounts for the effects of initial residual stress, yield stress, stress amplitude, and the number of cycles. They found that residual stresses on the surface are released more easily than those in the interior. Moreover, approximately 45%–60% of the maximum residual stress is released during the first cycle. Furthermore, the fatigue damage evolution of butt-welded joints under cyclic loading was studied by Shen et al. (2017) using the continuous damage mechanics approach. They suggested that the welding residual stress is released most significantly during the first loading cycle. Yi and Lee (2017) reached the same conclusion as Shen. Shen et al. (2021) further studied the release pattern of welding residual stress under cyclic loading and analyzed the fatigue life of a conical pressure vessel containing a semi-elliptical surface crack using the extended McEvily fatigue crack propagation rate model. Meanwhile, Dehkordi and Anaraki (2020) discovered that residual stress release is highly dependent on plasticity behavior. Their findings indicate that the isotropic hardening with nonlinear kinematic hardening model is more suitable for predicting stress relaxation than the perfect plasticity without hardening model in welded aluminum plates under cyclic loading. However, existing fatigue life analyses of welded components often ignore the influence of welding residual stress redistribution during crack propagation. Therefore, a coupled analysis of welding residual stress redistribution and crack propagation is crucial for accurately predicting the fatigue life of welded structures.

Thus far, the primary research methods for describing the welding residual stress redistribution with crack propagation include the empirical formula method and finite element method. Terada (2011) established the relationship equation between the welding residual stress field and fatigue crack propagation leveraging experimental data. Mukhtar (2013a, 2013b) described the relationship between welding residual stress and crack size in linear and polynomial forms and then analyzed the fatigue crack propagation of T-joint welded connections using the weight function method. Sutton et al. (2006) reconstructed the complete residual stress tensor field from the measured residual stress data. They proposed a hybrid approach for assessing the impact of residual stress on fatigue crack propagation and further investigated the effect of residual stress redistribution on the stress intensity factor (SIF) at the crack tip. Xu (2013) calculated the SIF during residual stress redistribution after crack propagation in welded plates using the finite element method. Then, they predicted the fatigue life using the principle of elastic superposition and the Forman formula. Shiue et al. (2004) extensively evaluated the effect of welding residual stress on the laser-surface-annealed AISI 304 stainless steel redistribution ahead of the crack tip. Noghabi et al. (2021) found that fatigue loads with different stress ratios influence the initial residual stress release. Greater stress ratio values increase the release rate of residual stress. They also conducted fatigue crack growth experiments (Noghabi et al., 2024) on compact tension samples fabricated from an aluminum alloy containing welding residual stresses. The results demonstrated the significant influence of residual stresses on fatigue crack propagation in these specimens. Yu et al. (2022) discovered that the influence of residual stress on fatigue life converges when residual stress reaches a certain level. The literature elucidated the patterns of crack propagation and welding residual stress redistribution, primarily focusing on empirical formula fitting and finite element method. However, the mutual effect between cracks and welding residual stress during the crack propagation process was still ignored.

The traditional analysis of fatigue crack propagation requires re-meshing repeatedly in the crack tip region, causing difficulty in the input of welding residual stress fields. However, this issue can be solved by the XFEM. The extended finite element theory was proposed by Belytschko (1999), allowing cracks to penetrate elements, rendering the re-mesh at the crack tip during crack propagation unnecessary. Consequently, the computational efficiency becomes highly improved. He (2019) carried out the prediction of crack paths on a 3D model using the XFEM. They observed that the results from the 3D model were closer to experimental data than those from a 2D model. Jie et al. (2020, 2022) used the Paris law and the XFEM to predict the fatigue life of cruciform joints. Their findings demonstrated the feasibility of employing the XFEM for predicting the fatigue life of complex structures.

Building on our earlier research into the release of welding residual stress under cyclic loading using a nonlinear follow-up hardening model, we found that the most significant release occurred within the initial 50 cycles. Figure 1 illustrates the mechanisms of welding residual stress release during the cyclic loading and unloading processes. However, this investigation (Shen et al., 2021) was conducted under the premise of excluding fatigue crack propagation effects. Hence, this paper investigates the variation of welding residual stress with crack propagation based on XFEM. In this study, welding residual stress was examined using numerical simulation. Subsequently, a numerical simulation of a tensile test was conducted to analyze the redistribution of residual stresses during crack propagation. On this basis, an extended finite element analysis method was proposed, incorporating the redistribution of welding residual stress for predicting crack propagation life. It provided an efficient analysis method for fatigue crack propagation of welded structures.

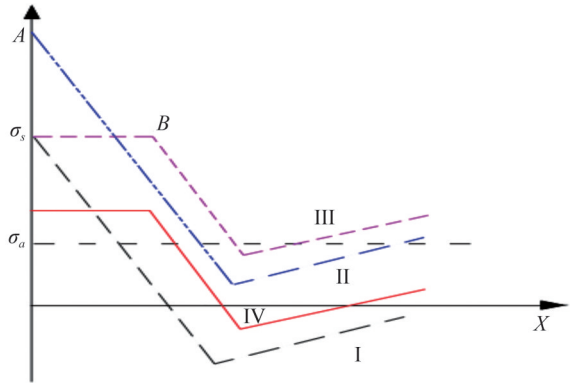

Figure 1 Mechanism of welding residual stress release

2 Fatigue crack propagation analysis method

2.1 Extended finite element method

The theory of extended finite elements was first introduced by Belytschko (1999). This method represents the discontinuity at the crack by introducing enriched functions. These enrichment functions comprise the asymptotic crack tip functions, which account for the singularity at the crack tip, and a discontinuous function that depicts the gap between the crack surfaces, as shown in Figure 2. The displacement approximation function is provided by Belytschko (1999) as follows:

$$\boldsymbol{u}(x) = \sum_{\mathbf{i} \in S} N_{\mathbf{i}}(x)\boldsymbol{u}_{\mathbf{i}} + \sum_{\mathbf{i} \in S_{\mathbf{h}}} N_{\mathbf{i}}(x)H(x)\boldsymbol{a}_{\mathbf{i}} + \sum_{\mathbf{i} \in S_{\mathbf{c}}} N_{\mathbf{i}}(x) \sum_{a=1}^{4} F_{\mathbf{a}}(x)\boldsymbol{b}_{\mathbf{i}}^{a} \tag{1}$$

where $N_{\mathbf{i}}(x)$ denotes shape functions, S indicates the node set in the finite element space, $S_{\mathbf{h}}$ refers to the set of nodes enriched with the discontinuous function, and $S_{\mathbf{c}}$ represents the node set with crack tip enrichment functions. $\boldsymbol{u}_{\mathbf{i}}$ illustrates the vector of nodal displacement, $F_{\mathbf{a}}(x)$ defines the asymptotic crack tip function, $\boldsymbol{a}_{\mathbf{i}}$ and $\boldsymbol{b}_{\mathbf{i}}$ denote the nodal enriched degree of freedom vector, and $H(x)$ indicates the discontinue jump function.

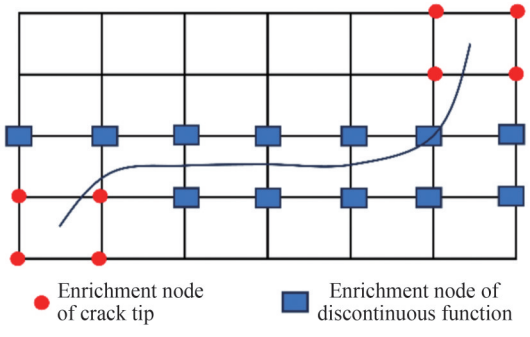

Figure 2 Enriched node distribution

For a general coordinate system of the crack, $H(x)$ is defined as follows (Belytschko, 1999):

$$H(x) = \begin{cases} 1 & (x - x^*) \cdot n \geqslant 0 \\ -1 & (\boldsymbol{x} - x^*) \cdot n \leqslant 0 \end{cases} \tag{2}$$

where x^* indicates the closest point on the crack to x, and n represents the outward normal vector in point x^*.

The asymptotic crack tip function for an isotropic material is defined as follows (Belytschko, 1999):

$$F_{\mathbf{a}}(x) = \left[\sqrt{r}\sin\frac{\theta}{2}, \sqrt{r}\cos\frac{\theta}{2}, \sqrt{r}\sin\theta\sin\frac{\theta}{2}, \sqrt{r}\cos\theta\cos\frac{\theta}{2}\right] \tag{3}$$

where r and θ refer to the local polar coordinates at the crack tip.

2.2 Extended McEvily model

The fatigue crack propagation rate curve is considered a key factor in predicting crack propagation life. The Paris law, proposed by Paris and Erdogan in 1963, describes the liner portion of the crack propagation rate curve and is expressed as follows:

$$\frac{\mathrm{d}a}{\mathrm{d}N} = C \cdot (\Delta K)^m \tag{4}$$

where ΔK indicates the SIF range, and C and m represent the material constants.

However, the Paris law can only describe the liner portion of the fatigue crack rate curve and does not account for the effects of load ratio, load sequence, threshold region, and unstable propagation. To address these limitations, the McEvily model was proposed by McEvily and Minakawa (1984) to consider the above issues. They introduced the following modified constitutive relationship for fatigue crack propagation, as follows:

$$\frac{\mathrm{d}a}{\mathrm{d}N} = A \cdot \left(\Delta K_{\mathrm{eff}} - \Delta K_{\mathrm{effth}}\right)^2 \tag{5}$$

$$\Delta K_{\mathrm{eff}} = K_{\mathrm{max}} - K_{\mathrm{op}} \tag{6}$$

$$K_{\mathrm{op}} = \left(1 - \mathrm{e}^{-ka}\right) \cdot \left(K_{\mathrm{opmax}} - K_{\mathrm{min}}\right) \tag{7}$$

where A refers to a material and environmentally sensitive constant, ΔK_{eff} indicates the effective range of SIF, $\Delta K_{\mathrm{effth}}$ represents the effective range of SIF at the threshold level, K_{op} denotes the SIF at the opening level for a macroscopic crack, k corresponds to a material constant, implying the rate of crack closure development with crack advance.

The McEvily formula was improved by Wang et al. (2008): the original fixed slope method in the formula was

modified to a variable slope method for different experimental conditions. In addition, the concept of virtual strength was used to replace the material's yield strength. The overload and underload parameters are introduced to describe the delayed crack propagation and acceleration effects. The SIF at the crack opening level and fracture toughness are considered functions related to crack length, integrating the three stages of crack propagation. The extended McEvily model can be expressed as follows:

$$\frac{\mathrm{d}a}{\mathrm{d}N} = \frac{A\left[K_{\max}\left(1 - f_{\mathrm{op}}\right) - \Delta K_{\mathrm{effth}}\right]^{m}}{1 - \left(K_{\max}/K_{\mathrm{c}}\right)^{n}} \tag{8}$$

where

$$\begin{cases} K_{\max} = \sqrt{\pi r_{\mathrm{e}}\left(\sec\dfrac{\pi\left|\sigma_{\max}\right|}{2\sigma_{\mathrm{V}}} + 1\right)}\left[1 + Y(a)\sqrt{\dfrac{a}{2r_{\mathrm{e}}}}\right]\sigma_{\max} \\ K_{\min} = \sqrt{\pi r_{\mathrm{e}}\left(\sec\dfrac{\pi\left|\sigma_{\min}\right|}{2\sigma_{\mathrm{V}}} + 1\right)}\left[1 + Y(a)\sqrt{\dfrac{a}{2r_{\mathrm{e}}}}\right]\sigma_{\min} \\ \Delta K = K_{\max} - K_{\min} \end{cases}$$

$$f_{\mathrm{op}} = \begin{cases} \max\left\{R, A_0 + A_1 R + A_2 R^2 + A_2 R^3\right\} & 0 \leqslant R < 1 \\ A_0 + A_1 R & -2 \leqslant R < 0 \end{cases}$$

$$\begin{cases} A_0 = \left(0.825 - 0.34\alpha' + 0.05\alpha'^2\right)\cdot\left[\cos\left(\pi\sigma_{\max}/2\sigma_{\mathrm{fl}}\right)\right]^{1/\alpha'} \\ A_1 = \left(0.415 - 0.071\alpha'\right)\cdot\sigma_{\max}/\sigma_{\mathrm{fl}} \\ A_2 = 1 - A_0 - A_1 - A_3 \\ A_3 = 2A_0 + A_1 - 1 \\ \sigma_{\mathrm{fl}} = \left(\sigma_{\mathrm{y}} + \sigma_{\mathrm{u}}\right)/2 \\ \alpha' = \dfrac{1}{1-2v} + \dfrac{1 - \dfrac{1}{1-2v}}{\left[1 + 0.886\,1\cdot\left(t/\left(K_{\max}/\sigma_{\mathrm{y}}\right)^{2}\right)^{3.225\,1}\right]^{0.759\,52}} \end{cases}$$

where parameters A and m are material and environmental influences, which can be obtained by experimental data fitting; f_{op} indicates the crack opening level function; $\Delta K_{\mathrm{effth}}$ denotes the effective range of the SIF at the threshold level; K_{c} refers to the fracture toughness of a material; $K_{\max}$ represents the maximum SIF; $K_{\min}$ corresponds to the minimum SIF; $Y(a)$ is a geometrical factor; r_{e} refers to an empirical material constant of the inherent flaw length of the order of 1 μm; σ_{v} indicates virtual strength of the material; R denotes stress ratio; α' is a crack tip stress/strain constraint ratio; $\sigma_{\max}$ denootes maximum applied stress; $\sigma_{\min}$ refers to minimum applied stress; σ_{fl} represents the flow stress; v is Poisson's ratio; σ_{y} corresponds to yield strength of the material, σ_{u} is the ultimate strength of the material.

2.3 Crack propagation life prediction method considering the mutual effect of welding residual stress redistribution and crack propagation

The XFEM module in Abaqus/CAE supports fatigue crack propagation calculations for 3D elements. However, this module regards the Paris law as the fatigue crack propagate rate model, which is not well-suited for complex loading conditions. Consequently, a method based on the extended McEvily model for extended finite element analysis is proposed using Abaqus secondary development technology. The analysis procedure is illustrated in Figure 3.

The program primarily consists of two modules: the welding module, which uses the welding DFLUX subroutine written in Fortran to solve the temperature and stress fields simulating the welding process. The resulting stress field is then employed as the initial state in the crack propagation model. The fatigue crack propagation calculation module is developed using Python within the framework of Abaqus secondary development. It determines the SIF at the crack tip, considering the combined effects of cyclic fatigue loading and welding residual stresses. The next propagation length is ascertained using equation (8), followed by the recalculation of the welding residual stress field. The process continues until either the critical crack length is reached or the maximum SIF at the crack tip exceeds the fracture toughness.

Compared with traditional methods, the proposed approach is well-suited for analyzing crack propagation under welding residual stress states. As the crack propagates, the stress state from the previous step is carried over to the next. The welding residual stress is updated at each calculating step of crack propagation, and the updated welding residual stress will be superimposed with fatigue load, forming the new stress field for the subsequent step of crack propagation.

3 TC4 plate welding test

In this section, the direct coupling method is used to calculate welding residual stresses. This approach employs temperature–stress coupling elements to simultaneously solve the temperature field and stress field. The DFLUX subroutine, written in FORTRAN, is used to simulate the double-ellipsoid moving heat source during welding. The initial temperature is set at 25 ℃, with a material Poisson's ratio of 0.34 and a convective heat transfer coefficient of 50 W/(m^2 ℃). Due to the thin plate thickness of the welded component, a single-pass welding with a weld seam width of 6 mm is simulated. Additional welding parameters are listed in Table 1 (Yan et al., 2018). The thermal and mechanical properties of TC4 titanium alloy varying with temperature are shown in Figure 4 (Li, 2006), with the transition temperature of the TC4 ranging from 1 600 ℃ (solidus) to

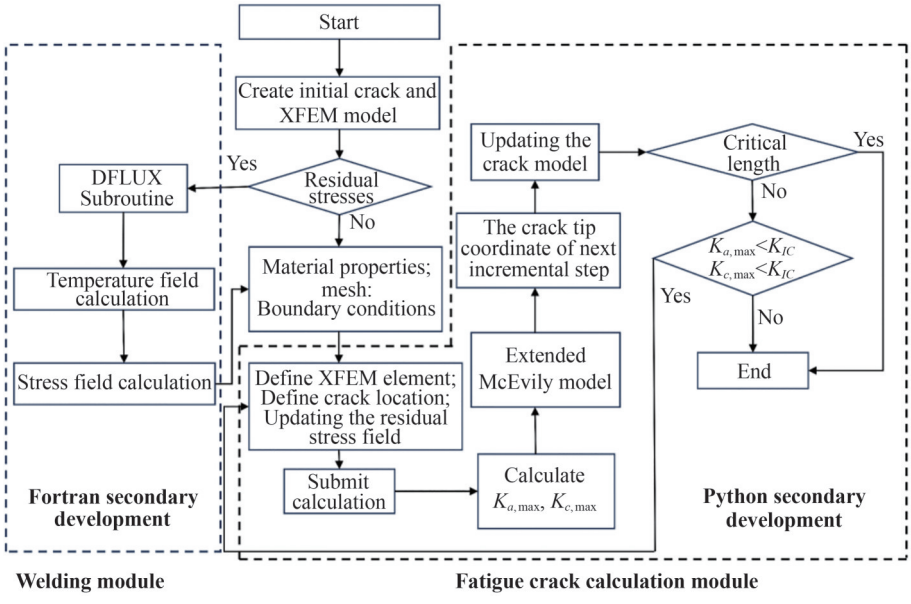

Figure 3 Crack propagation life analysis method considering the mutual effect of residual stress redistribution and crack propagation

Table 1 Welding-related parameters of the test piece (Yan et al., 2018)

Test piece	I (A)	U (V)	Weld speed (mm/s)	Number of weld seams
TC4 plate	70	15	1.5	1

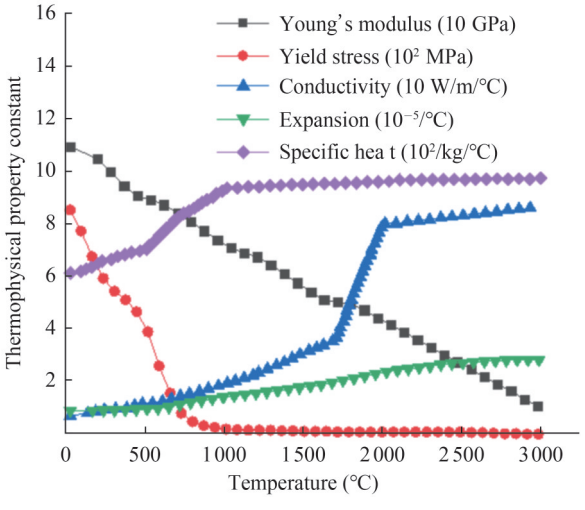

Figure 4 Temperature-dependent material properties of TC4 (Li et al., 2006)

1660 °C (liquidus).

The TC4 plate welding test specimen measures 50 mm in width, 30 mm in length, and 3 mm in thickness. The weld seam with a width of 6 mm is positioned at the center of the TC4 plate, as shown in Figure 5. This process involves constraining the linear displacements of the four corner points (Yan et al., 2018) of the butt-welded flat plate, as shown in Figure 6.

During the welding process, the welding pool, representing the highest temperature region of the moving heat source, has a maximum temperature of 2495 °C, as shown in Figure 7. As the heat source moves, heat continuously diffuses from the welding pool to both sides of the base material. Currently, the welding heat-affected zone continuously expands with increasing time.

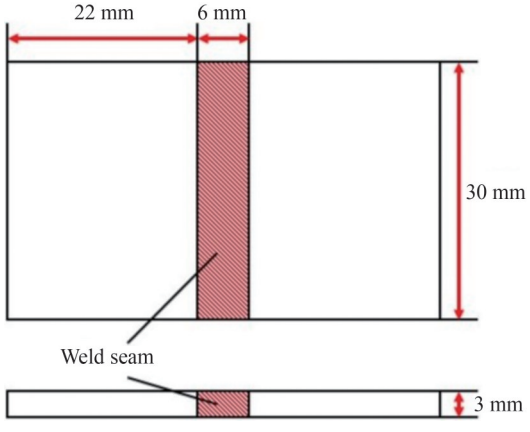

Figure 5 TC4 plate welding dimensions

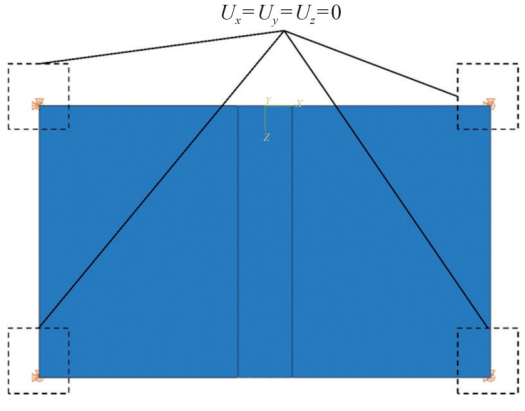

Figure 6 Boundary conditions

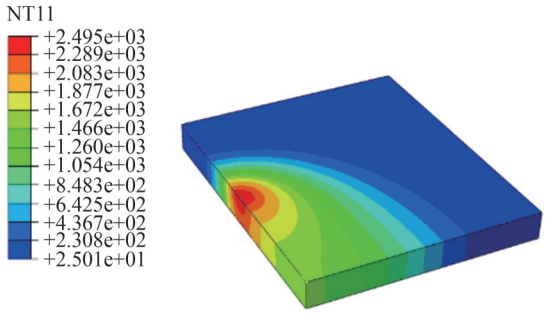

Figure 7 Distribution of welding temperature field during the welding process (half width)

The welding residual stress in the plate is shown in Figure 8. The lateral welding residual stress is mainly tensile stress, and it reaches a maximum value in the center area of the plate. The lateral welding residual stress and longitudinal welding residual stress of this butt-welded plate are extracted along path 1 to quantitatively study the distribution of welding residual stress, as shown in Figure 9.

On path 1, the lateral welding residual stress exhibits a double-peak distribution, with two "peaks" positioned on either side of the weld seam. The peak tensile stress reaches 160 MPa, accounting for 17% of the material's yield strength. On the contrary, the longitudinal welding residual stress displays a single peak distribution. The maximum tensile stress is 355 MPa, representing 39% of the material's yield strength. Beyond the weld seam, this stress transitions into compressive stress, reaching 365 MPa, which is 40% of the material's yield strength.

As shown in Figure 9, the numerical calculation results exhibit a distribution trend that closely aligns with the welding test results determined by the X-ray diffraction method (Yan et al., 2018) for the TC4 butt-welded plate. Hence, the direct coupling method of welding numerical simulation is an appropriate method.

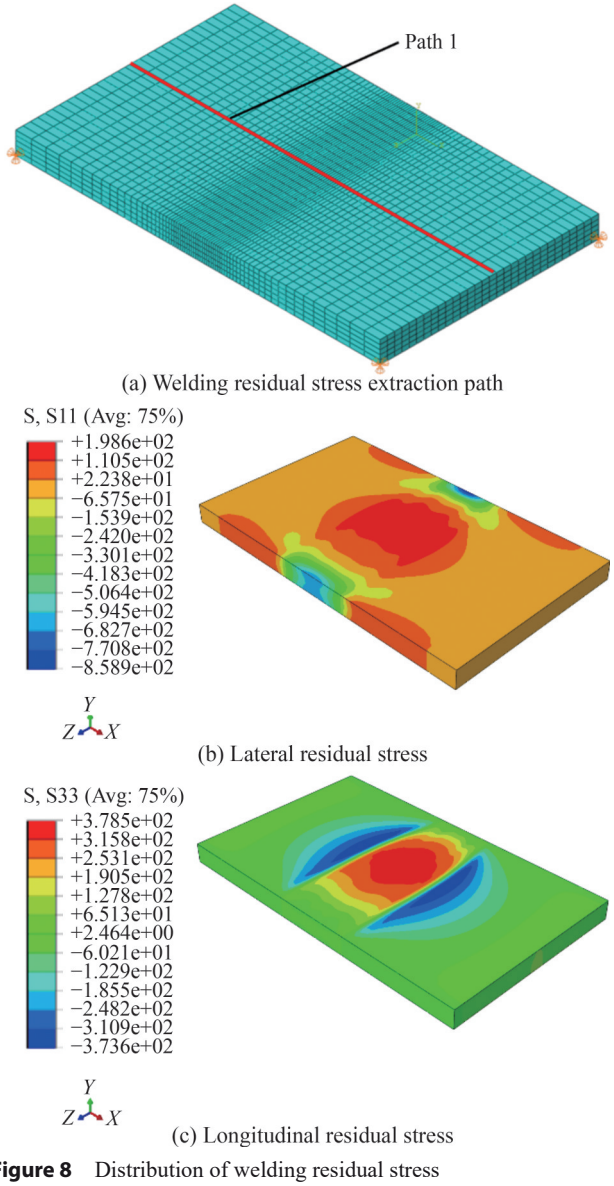

Figure 8 Distribution of welding residual stress

4 TC4 plate with semi-elliptical surface crack

4.1 3D XFEM model

A tensile fatigue test specimen XFEM model is developed using Abaqus/CAE. The model represents a rectangular TC4 plate of 132 mm × 18 mm × 4 mm. To balance computational efficiency and accuracy, the region near the crack is finely meshed, whereas other areas are coarsely meshed, as shown in Figure 10.

Considering a semi-elliptical surface crack at the center, the model is subjected to cyclic tensile loading. Rigid fixed boundary conditions are applied to the lower end of the model. Meanwhile, the upper end is constrained in the X and Z directions for displacement and in the X, Y, and Z directions for rotation. The boundary condition is shown in Figure 11.

4.2 Mesh size sensitivity analysis for SIF calculation

Mesh size sensitivity analysis is conducted to determine the required fineness of the mesh. The analysis is mainly divided into two parts: the integral contour influence and the mesh size influence.

In the analysis of integral contour influence, five different contours are set to calculate the SIF of the crack tip, with a minimum mesh size of 0.1 mm. In the analysis of the mesh size influence, the minimum mesh sizes in the crack propagation region are set within the range of 0.1–0.5 mm, based on the results from the fifth contour.

In the sensitivity analysis, the semi-elliptical surface crack has a half-width (c) of 2.1 mm, a depth (a) of 1.4 mm, and is subjected to a maximum tensile load of 500 MPa. The

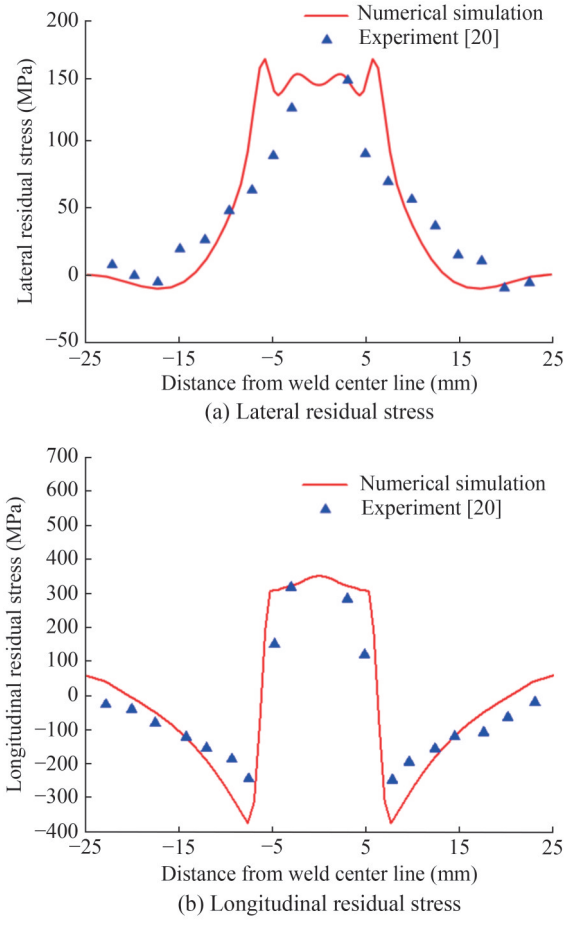

Figure 9 Welding residual stress distribution for path 1

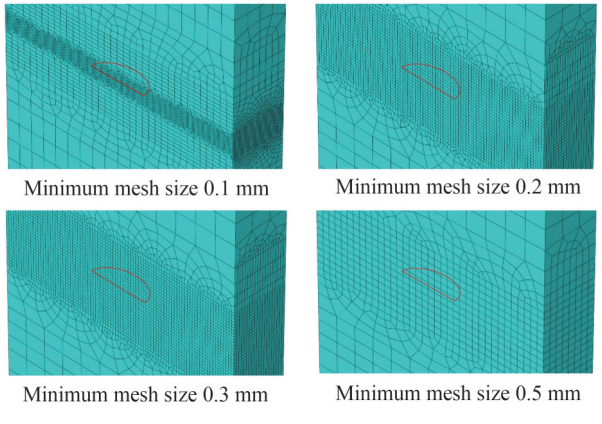

Figure 10 Mesh size

SIFs at the crack tip (at the crack depth end) are extracted from the Abaqus output, as shown in Figure 12. These SIFs are compared with the results computed using the Newman–Raju empirical formulas to determine the optimal mesh size and the most suitable contour.

The SIF results of the crack tip are presented in Figure 12. In the analysis of integral contour influence, the first contour reveals a large deviation between the SIF calculated using Abaqus and the results obtained from the Newman–Raju method. However, from the third to the fifth contour, this deviation is minimized and stabilizes. In the analysis of mesh size influence, the results show that the SIF is also influenced by the mesh size. As the mesh size is reduced to 0.2 mm, the SIF deviation gradually decreases and stabi-

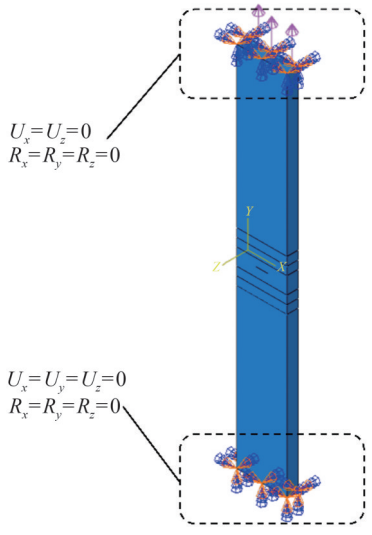

Figure 11 Boundary condition

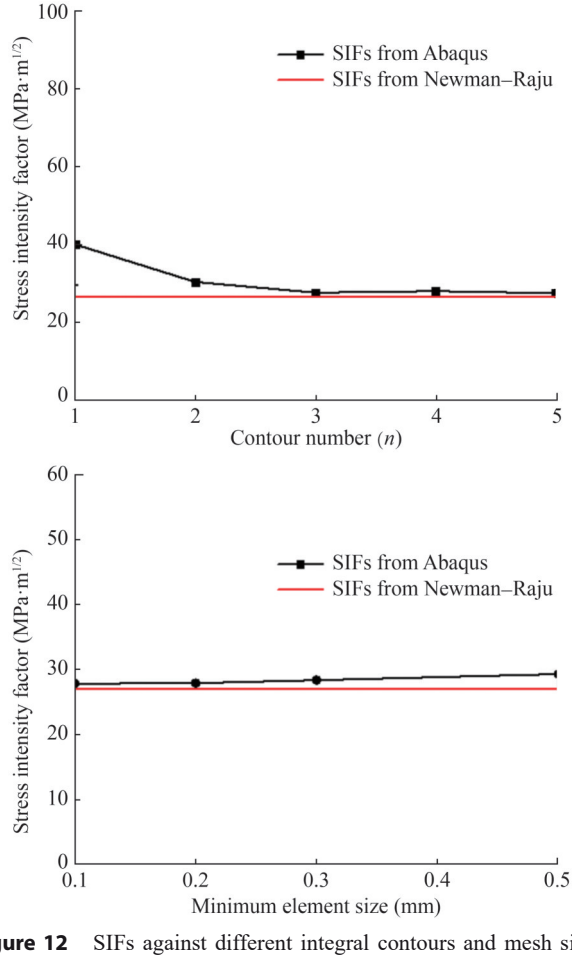

Figure 12 SIFs against different integral contours and mesh sizes at depth end

lizes. Therefore, considering computational efficiency, the minimum mesh size is set to 0.2 mm for the subsequent calculations using the fifth contour.

5 Mutual influence analysis of welding residual stress redistribution and crack propagation

5.1 Parameter determination in the extended McEvily model

The parameters in the extended McEvily formula can be obtained by fitting the experimental fatigue crack propagation rate curve. The extended McEvily formula is shown in equation (9) as follows:

$$\frac{\mathrm{d}a}{\mathrm{d}N}=\frac{A\left[K_{\max}\left(1-f_{\mathrm{op}}\right)-\Delta K_{\mathrm{effth}}\right]^{m}}{1-\left(K_{\max}/K_{\mathrm{c}}\right)^{n}} \tag{9}$$

The experimental data (Wu, 2022) suggest that the fracture toughness of the TC4 alloy is $\Delta K_{\mathrm{c}}=270\ \mathrm{MPa}\cdot\sqrt{\mathrm{m}}$. The threshold SIF for TC4 alloy at $R=0.1$ is $\Delta K_{\mathrm{th}}=5.29\ \mathrm{MPa}\cdot\sqrt{\mathrm{m}}$ (Wang et al., 2021). These data are substituted in equation (10) as follows:

$$\Delta K_{\mathrm{effth}}=K_{\max}\left(a_{\mathrm{th}}\right)\left[1-f_{\mathrm{op}}\left(a_{\mathrm{th}}\right)\right] \tag{10}$$

Then, the threshold value of the effective SIF $\Delta K_{\mathrm{effth}}=4.41\ \mathrm{MPa}\cdot\sqrt{\mathrm{m}}$.

The parameters A and m in equation (9) can be obtained as follows. Initially, the extended McEvily formula is transformed into the following form:

$$\frac{\mathrm{d}a}{\mathrm{d}N}\left[1-\left(K_{\max}/K_{\mathrm{c}}\right)^{n}\right]=A\left[K_{\max}\left(1-f_{\mathrm{op}}\right)-\Delta K_{\mathrm{effth}}\right]^{m} \tag{11}$$

By integrating $H=K_{\max}\left(1-f_{\mathrm{op}}\right)-\Delta K_{\mathrm{effth}}$, equation (12) is acquired as follows:

$$\frac{\mathrm{d}a}{\mathrm{d}N}\left[1-\left(K_{\max}/K_{\mathrm{c}}\right)^{n}\right]=A\cdot H^{m} \tag{12}$$

Equation (13) is obtained by taking the logarithm of both sides of equation (12) as follows:

$$\log\left\{\frac{\mathrm{d}a}{\mathrm{d}N}\cdot\left[1-\left(K_{\max}/K_{\mathrm{c}}\right)^{n}\right]\right\}=\log A+m\cdot\log H \tag{13}$$

Thus, the relationship curve can be plotted with $\log\left\{\frac{\mathrm{d}a}{\mathrm{d}N}\cdot\left[1-\left(K_{\max}/K_{\mathrm{c}}\right)^{n}\right]\right\}$ and $\log H$ as the coordinate axes. The material parameters A and m can be obtained through linear fitting, given the linear relationship between the two terms.

The crack propagation rate curve under the stress ratio R of 0.1 for the TC4 plate with thickness B = 4 mm is shown in Figure 13. The fitted fatigue crack propagation rate curve based on the extended McEvily model aligns well with the experimental data from Wu (2022), enabling accurate calculation of the three stages of fatigue crack propagation.

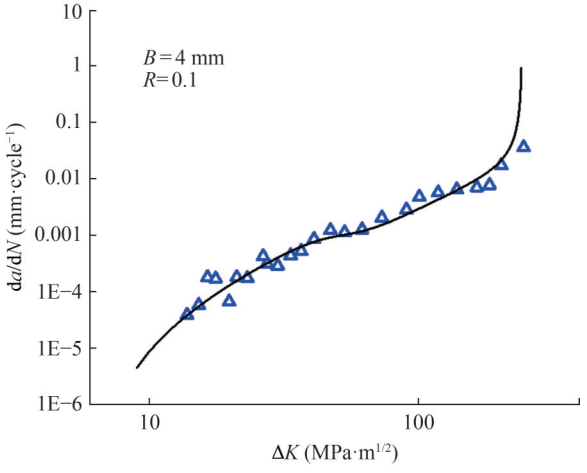

Figure 13 Crack propagate rate curve fitting

The extended McEvily formula for the stress ratio R = 0.1 after fitting is shown in equation (14) as follows:

$$\frac{\mathrm{d}a}{\mathrm{d}N}=\frac{9.209\,16\times10^{-7}\left[K_{\max}\left(1-f_{\mathrm{op}}\right)-4.41\right]^{2.083\,42}}{1-\left(K_{\max}/270\right)^{6}} \tag{14}$$

where $K_{\max}$ refers to the maximum SIF under cyclic loading, and f_{op} indicates the crack opening function.

The tension ability of TC4 titanium alloy is illustrated in Figure 14, where the yield stress is 860 MPa.

5.2 Welding residual stress calculation

This process involves constraining the linear displacements of the four corner points of the butt-welded flat plate, as depicted in Figure 15. The weld seam, with a width of 6 mm and a length of 18 mm, is positioned at the center of the flat plate, as shown in Figure 16.

The welding heat source moves from left to right. When the welding process is complete, it naturally cools down to room temperature. The welding residual stresses in the Y-direction (lateral welding residual stresses) are extracted along Paths 1 and 2 of the weld seam. Figure 17 shows the distribution of lateral welding residual stresses.

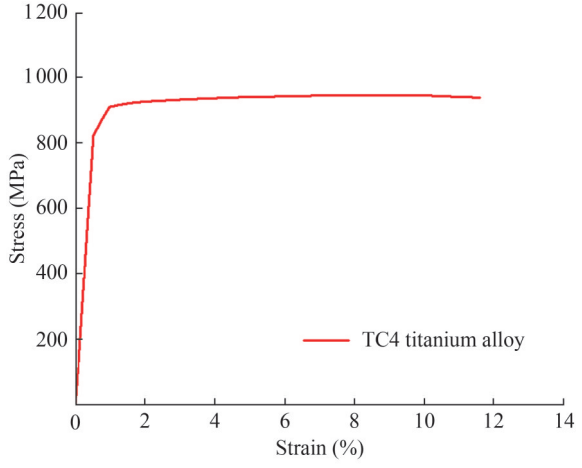

Figure 14 TC4 titanium alloy tension ability

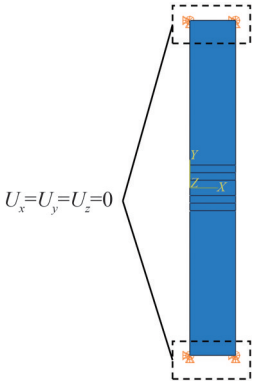

Figure 15 Boundary condition of welding

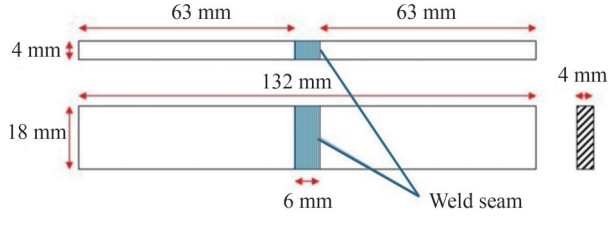

Figure 16 Welding specimen and welding position

As observed in Figure 18, along this path, the lateral welding residual stresses exhibit a distribution pattern of compressive stress-tensile stress-compressive stress. The compressive stress is evident in the welding arc initiation region (the start of the weld). The tensile stress is observed at the center of the flat plate, reaching a peak tensile stress of 83 MPa. Another compressive stress region is presented in the area near the right end face (the end of the weld).

Shiue et al. (2004) suggested that welding residual tensile stresses have a significant impact on the rate of fatigue crack propagation. Therefore, the central region of the flat plate with higher levels of tensile stress is identified as the critical area for fatigue crack initiation. In subsequent calculations, the initial crack is assumed to be positioned in this region.

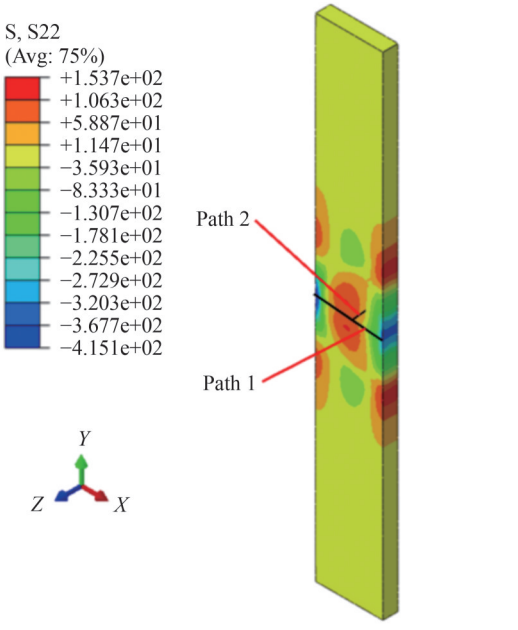

Figure 17 Path of the heat source and the lateral welding residual stress distribution

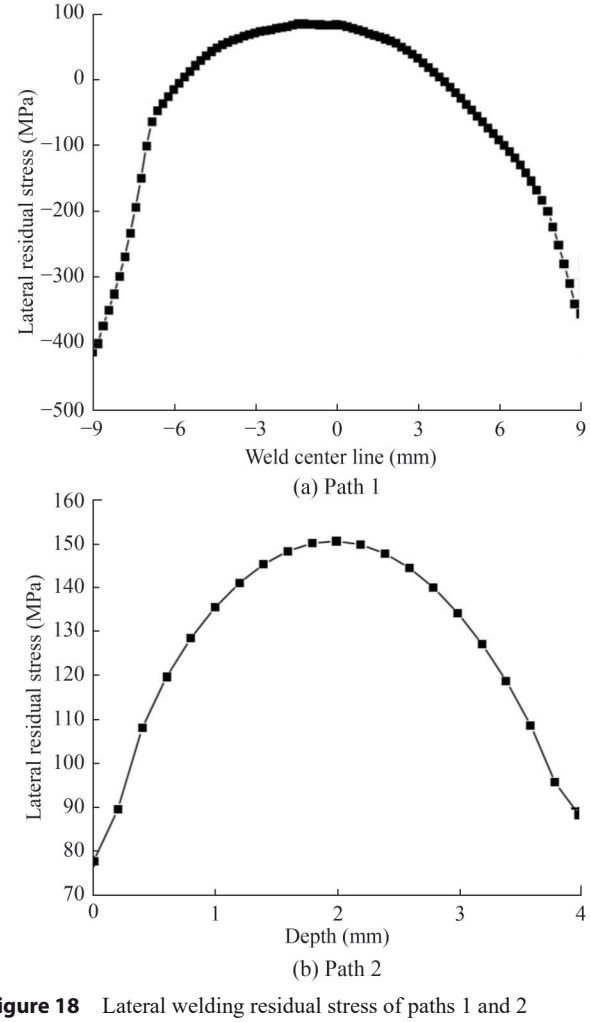

Figure 18 Lateral welding residual stress of paths 1 and 2

5.3 Fatigue crack propagation coupling with the welding residual stress

The initial crack exhibits a surface crack with a length of $2c = 4.2$ mm and a depth of $a = 1.5$ mm. The maximum fatigue cyclic load is set to 250 MPa, with a load ratio of $R = 0.1$, as shown in Figure 19. The boundary conditions are the same as those in Section 4.1. The extended McEvily model has been determined in Section 5.1, and the fatigue crack propagation calculation process is shown in Figure 2. To investigate the influence of welding residual stress redistribution on the crack propagation rate, three distinct conditions are designed for comparison, as outlined in Table 2. In condition 1, welding residual stress is not considered. In condition 2, the welding residual stress field calculated in Section 5.2 is set as the initial state, considering the welding residual stress and its redistribution. The traditional method is applied in condition 3 and compared with condition 2, and the welding residual stress as a constant is incorporated into the tensile fatigue specimen model for fatigue crack propagation analysis using the load superposition method. Hou (1990) suggested that the magnitude of welding residual stress equates to 0.3 σ_y.

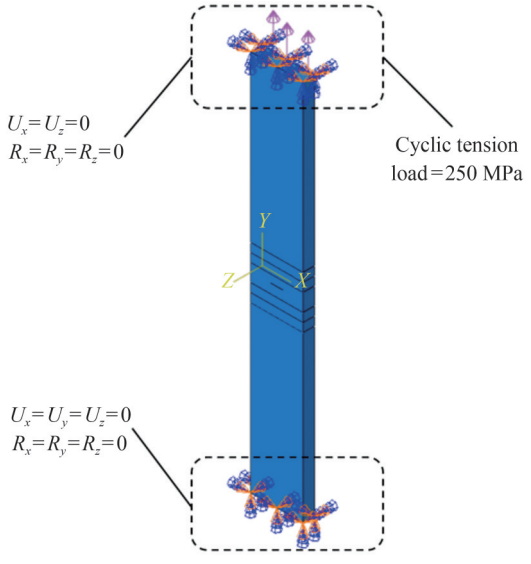

Figure 19 Boundary condition and fatigue load

Table 2 Conditions of calculation

Conditions	Values of welding residual stress
1	Without the welding residual stress
2	Welding residual stress calculated in 5.2
3	Welding residual stress equals 0.3 σ_y

Surface crack propagation calculations involve tracking the maximum SIFs $K_{max,\,c}$ and $K_{max,\,a}$ at the crack tip in the length and depth directions for each cycle increment. The values of Δc and Δa are calculated for each cycle increment, and then the total crack length c and total crack depth a are obtained through iterative cycling. Using the crack length data at each cycle increment, the surface fatigue crack propagation morphology can be visualized.

According to the proposed fatigue crack propagation analysis method in Section 2.3, the stress distribution within the structure during the surface crack propagation process can be extracted. After each unloading of the fatigue load, the stress extracted from the structure represents the welding residual stress. The lateral welding residual stress is extracted according to the two different types of paths shown in Figure 20. Paths 1 to 8 trace the stress from the crack end to the edge of the plate, whereas Paths 1* through 7* represent the paths from the crack depth to the back of the plate thickness.

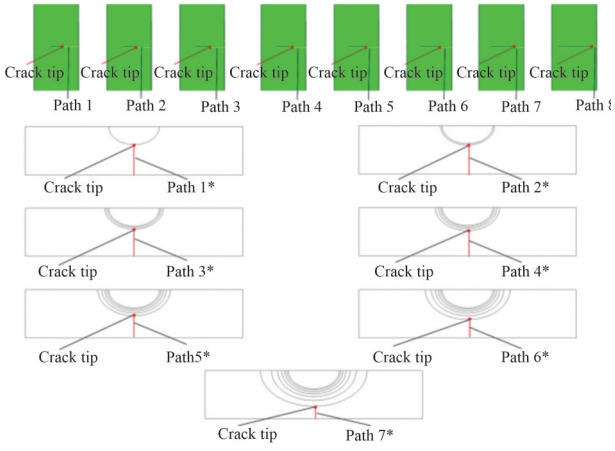

Figure 20 Welding residual stress extraction path

5.4 Results and discussion

The surface crack propagation morphology is illustrated in Figure 21. Under conditions 1 and 2, the crack propagation follows similar patterns, characterized by a smaller increment in the initial stage and a larger increment in the later stages. By contrast, under condition 3, the crack propagation increment is more uniform because crack propagation remains in the second stage of fatigue crack propagation. In conditions 1 and 2, the crack tip SIF is near the threshold value in the initial stages of crack propagation, leading to a smaller increment in crack propagation.

Under all three conditions, crack propagation occurs perpendicular to the direction of the tensile load. The crack morphology appears as a semi-ellipse and is symmetrically distributed, gradually propagating from the center toward the thickness of the plate and both sides.

The lateral residual welding stresses from the crack end to the edge of the plate and from the crack depth to the back of the plate under varying crack sizes for conditions 2 and 3 are extracted according to the paths in Figure 20. The distribution is shown in Figures 22 and 23. In these graphs, the zero point of the horizontal axis denotes the width cen-

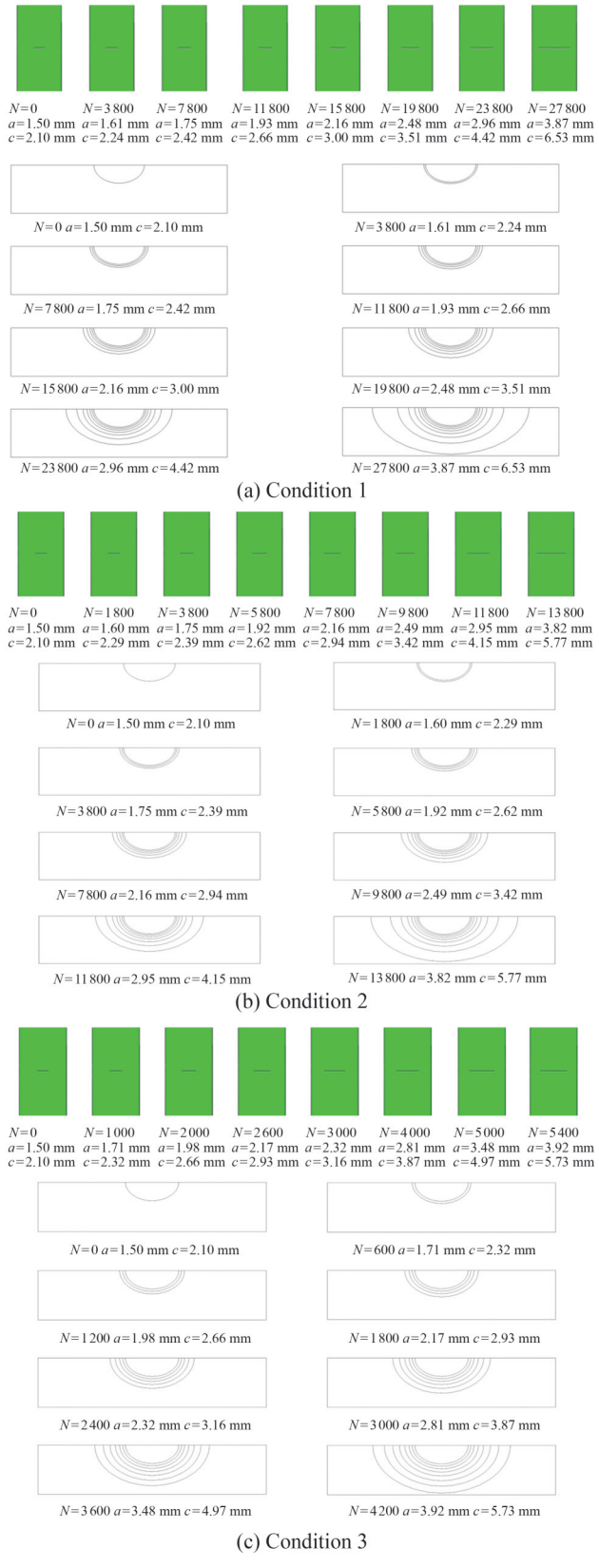

Figure 21 Surface crack propagation path and shape

ter of the plate's upper surface, and the first data point on the left side of each curve represents the lateral residual

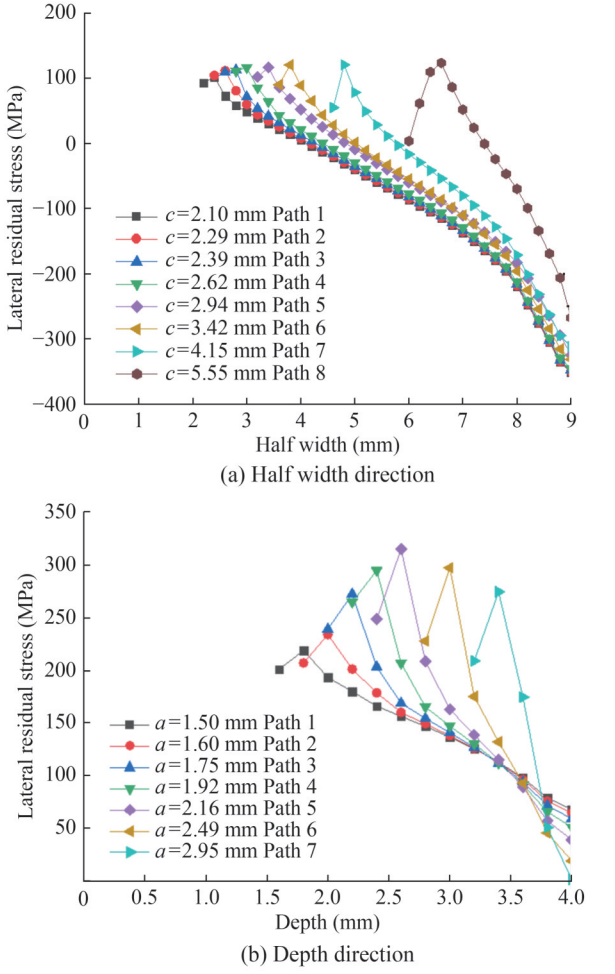

Figure 22 Welding residual stress distribution in front of the crack tip during crack propagation for working condition 2

welding stress at the crack tip.

Figure 22(a) illustrates the distribution of lateral residual welding stress corresponding to various crack sizes under condition 2. Each curve depicts the lateral residual welding stress distribution, extending from the crack end to the edge of the plate width for different crack sizes. As the crack progresses, the welding residual stress at the crack tip initially increases and then decreases. Moreover, the distribution pattern of each curve is nearly identical. The maximum lateral welding residual stress on the curve is not located at the crack tip but in the area close to the front of the crack tip. The welding residual stress gradually decreases with increasing distance from the crack tip, transitioning from tensile stress to compressive stress. This finding indicates that the welding residual stress near the crack tip region has been released.

Figure 22(b) illustrates the distribution of lateral welding residual stress from the crack depth to the back of the plate for various crack sizes under condition 2. The welding residual stress at the crack tip in the depth direction follows a pattern similar to that in the length direction as the

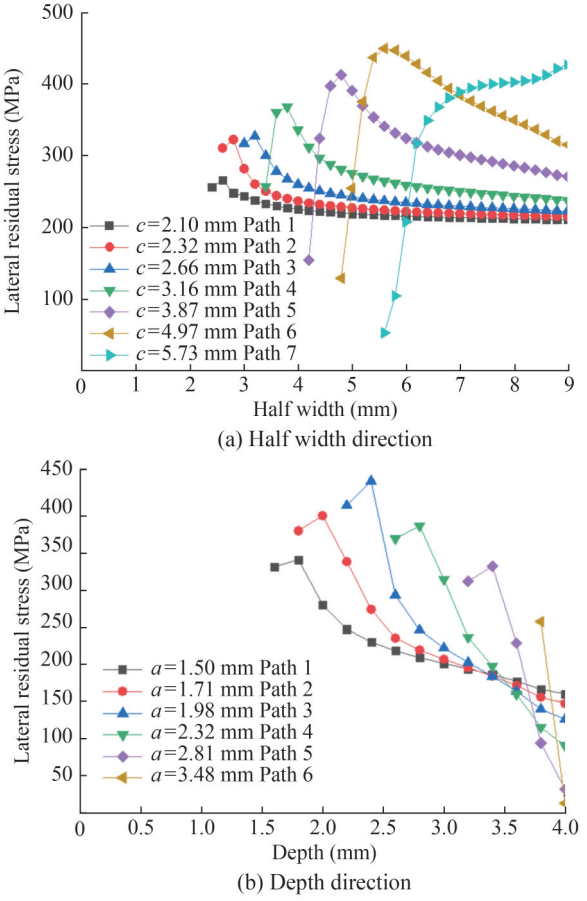

Figure 23 Welding residual stress distribution in front of the crack tip during crack propagation for working condition 3

crack propagates. However, the welding residual stress level at the back of the plate gradually decreases during crack propagation. This decline is attributed to the stress state transitioning from plane strain to plane stress in the back region of the plate as the crack depth increases, resulting in the release of welding residual stress.

Figure 23(a) demonstrates the distribution of lateral welding residual stress from the crack length end to the plate width end under condition 3. The residual stress level for condition 2 is higher than that in condition 3. As the crack propagates, the magnitude of residual stress at the crack tip in the length direction decreases to a low quantity, but it is still higher than that in condition 2. Hence, the SIF amplitude at the crack tip becomes larger than those of the two other conditions, leading to a higher crack propagation rate.

The lateral welding residual stress distribution from the crack depth to the back of the plate in working condition 3 resembles that of working condition 2, as shown in Figure 23(b). However, the residual stress level in working condition 3 is markedly higher than in working condition 2.

Figure 24 illustrates the relationship between the crack propagation life of TC4 specimens and the surface crack length c and depth a under three different working conditions. The figure demonstrated that the fatigue crack propagation rates for conditions 2 and 3 are higher than that for condition 1, implying that welding residual stresses increase crack propagation rate and decrease crack propagation life. Compared with that in condition 3, the fatigue crack propagation rate in condition 2 is relatively lower, leading to a longer cycling time. This phenomenon is due to the constant welding residual stress of 0.3 σ_y applied in condition 3. Condition 2 represents the welding residual stress distribution obtained using numerical welding simulation, where tensile and compressive stresses exist simultaneously. Furthermore, the redistribution of residual stresses is considered in the crack propagation calculation. Therefore, the computational results under condition 2 are more reasonable with the actual situation.

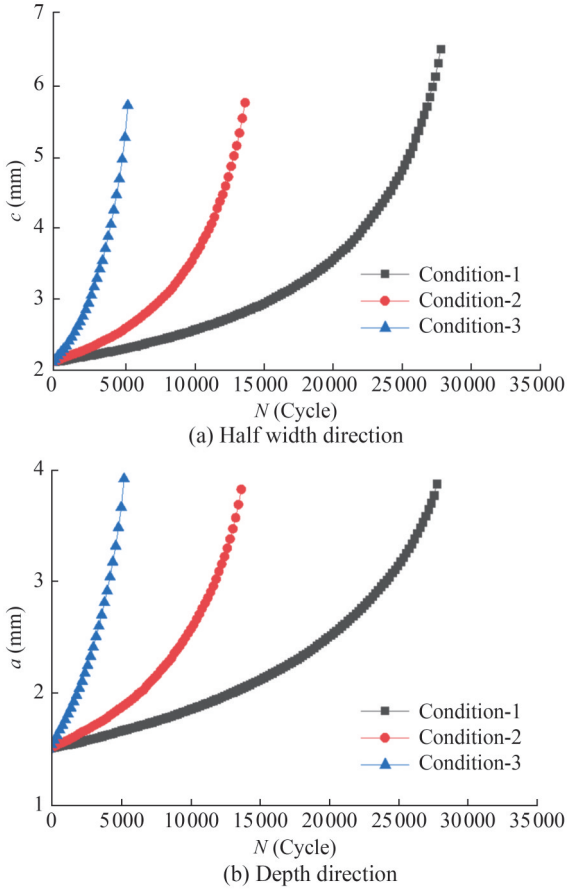

Figure 24 Variation of crack size against the number of load cycles

The summary of cycling time results under the three working conditions is presented in Table 3. The crack propagation life for condition 1, which ignores welding residual stress, is 201.4% of that for condition 2, suggesting that the prediction for condition 1 tends to be excessively aggressive. By contrast, the crack propagation life for condition 3 is only 39.1% of that for condition 2, indicating that regarding welding residual stress as a constant tensile stress of 0.3 σ_y in the prediction may lead to an overly conservative

prediction. Thus, the consideration of welding residual stress redistribution in condition 2 is more reasonable.

Table 3 Crack propagation life comparison

Conditions	Crack propagation life (cycle)	%
1	27800	201.4
2	13800	100
3	5400	39.1

6 Conclusions

A TC4 titanium alloy tensile fatigue specimen was selected as a case study to analyze the redistribution of welding residual stress during crack propagation using the XFEM. The variation patterns of welding residual stress redistribution in the crack tip region of the specimen and its crack propagation life were calculated. The following conclusions were drawn:

1) A crack propagation life prediction method, considering the mutual effects between welding residual stress redistribution and surface crack propagation, was proposed. An iterative calculation of fatigue crack propagation with the welding residual stress field was achieved using secondary development to Abaqus.

2) During crack propagation, the residual stress at the crack tip changes not only at the crack end but also along the crack depth. As the crack propagates, the lateral welding residual stresses at the crack end and along the crack depth exhibit a pattern of initially increasing and then decreasing trends.

3) As the crack propagates through the thickness of the plate, the stress state transitions from a plane strain state to a plane stress state. This transition reduces the lateral welding residual stress.

4) The crack propagation life of the TC4 butt-welded specimen, when ignoring welding residual stress, is 201.4% of that under the scenario with numerically simulated welding residual stress. On the contrary, when employing the load superposition method and regarding 0.3 σ_y as the welding residual stress, the crack propagation life is 39.1% of that under the scenario with numerically simulated welding residual stress. Both situations could result in excessively aggressive or overly conservative predictions of crack propagation life. The comparative analysis reveals that the proposed crack propagation life prediction method can provide more reasonable and accurate crack propagation life prediction for welded structures.

Nomenclature

$N_i(x)$	represents shape functions
S	is the node set in the finite element space
S_h	is the set of nodes enriched with the discontinuous function
S_c	is the node set with crack tip enrichment functions
u_i	is the vector of nodal displacement
$F_a(x)$	defines the asymptotic crack tip function
a_i, b_i	denote the nodal enriched degree of freedom vector
$H(x)$	is the discontinue jump function
x^*	is the closest point on the crack to x
n	is the outward normal vector in point x^*
r, θ	refer to the local polar coordinates at the crack tip
SIF	indicates the stress intensity factor
ΔK	is the SIF range
C, m	is the Paris constant
ΔK_{eff}	is the effective range of SIF
ΔK_{effth}	is the effective range of SIF at the threshold level
K_{op}	is the SIF at the opening level for a macroscopic crack
k	is a material constant, which represents the rate of crack closure development with crack advance
A, m	correspond to the material and environmental influence constants of the extended McEvily formula; can be obtained by experimental data fitting
f_{op}	is the crack opening level function
K_c	is the fracture toughness of a material
K_{max}	is the maximum SIF
K_{min}	is the minimum SIF
$Y(a)$	is a geometrical factor
r_e	is an empirical material constant of the inherent flaw length of the order of 1μm
σ_v	is virtual strength of the material
R	is the stress ratio
α'	is a crack tip stress/strain constraint ratio
σ_{max}	is the maximum applied stress
σ_{min}	is the minimum applied stress
σ_{fl}	is the flow stress
v	is Poisson's ratio
σ_y	is the yield strength of the material
σ_u	is the ultimate strength of the material

Funding The research reported in this paper is supported by the National Major Project.

Competing interest The authors have no competing interests to declare that are relevant to the content of this article.

References

Al-Mukhtar A (2013a) Consideration of the residual stress distributions in fatigue crack growth calculations for assessing welded steel joints. Fatigue & Fracture of Engineering Materials & Structures 36: 1352-1361. https://doi.org/10.1111/ffe.12060

Al-Mukhtar A (2013b) Residual stresses and stress intensity factor calculations in T-welded joints. Journal of Failure Analysis & Prevention 13: 619-623. https://doi.org/10.1007/s11668-013-9723-0

Belytschko T (1999) Elastic crack growth in finite elements with minimal remeshing. International Journal for Numerical Methods In Engineering 45: 601-620. https://doi. org/10.1002/(sici)1097-0207(19990620)45:5<601::aid-nme598>3.0.co;2-s

Dehkordi Y, Anaraki A (2020) Comparative study of the effective parameters on residual stress relaxation in welded aluminum plates under cyclic loading. Mechanics & Industry 21(5): 505. https://doi.org/10.1051/meca/2020061

He L (2019) Fatigue Crack Propagation path and life prediction based on XFEM. Journal of Northwestern Polytechnical University 37(4): 737-743. https://doi.org/10.3969/j.issn.1000-2758.2019.04.013 (in Chinese)

Hou W (1990) Prediction of crack growth rate of conical cylinder-combined shell structure in residual stress field. Ship Performance Research 4: 53-60 (in Chinese)

Jie Z, Wang W, Fang R, Zhuge P, Ding Y (2020) Stress intensity factor and fatigue analysis of cracked cruciform welded joints strengthened by CFRP sheets considering the welding residual stress. Thin–Walled Structures 154: 106818. https://doi.org/10.1016/j.tws.2020.106818

Jie Z, Wang K, Liang S (2022) Residual stress influence on fatigue crack propagation of CFRP strengthened welded joints. Journal of Constructional Steel Research 196:107443. https://doi.org/10.1016/j.jcsr.2022.107443

Li C (2006) China Materials Engineering Canon. Chemical Industry Press, Beijing (in Chinese)

Li L, Wang Z (2009) Fatigue strength correction formula of typical FPSO welded joint based on residual stress release. Journal of Ship Mechanics 13(1): 82-90. https://doi.org/10.3969/j.issn.1007-7294.2009.01.011 (in Chinese)

McEvily A, Minakawa K (1984) Crack closure and the growth of short and long fatigue cracks. Scripta Metall 18: 71–76. https://doi.org/10.1016/0036-9748(84)90092-9

Noghabi M, Sattarifar I, Toudeshky H (2021) The study of redistribution in residual stresses during fatigue crack growth. Journal of Mechanical Engineering and Sciences 15(4): 8565-8579. https://doi.org/ 10.15282/jmes.15.4.2021.09.0675

Noghabi M, Sattarifar I, Toudeshky H (2024) The impact of welding residual stresses on fatigue crack growth behaviour in aluminium alloy plates: a numerical and experimental investigation. Advances in Materials and Processing Technologies 1-20. https://doi.org/10.1080/2374068X.2024.2398785

Paris P, Erdogan F (1963) A critical analysis of crack propagation laws. Journal of Basic Engineering 528-533. https://doi.org/10.1115/1.3656900

Shen F, Zhao B, Li L (2017) Fatigue damage evolution and lifetime prediction of welded joints with the consideration of residual stresses and porosity. International Journal of Fatigue 103: 272-279. https://doi.org/10.1016/j.ijfatigue.2017.06.014

Shen Y, Luo G E, Jiang X W (2021) Fatigue life analysis considering welding residual stress release. Journal of Ship Mechanics 25(07): 935-945. https://doi.org/10.3969/j.issn.1007-7294.2021.07.011 (in Chinese)

Shiue R, Chang C, Young M (2004) The effect of residual thermal stresses on the fatigue crack growth of laser-surface-annealed AISI 304 stainless steels: Part I: computer simulation. Materials Science and Engineering 364: 101-108. https://doi.org/10.1016/j.msea.2003.07.003

Sutton M, Reynolds A, Ge Y (2006) Limited weld residual stress measurements in fatigue crack propagation : Part II. FEM-based fatigue crack propagation with complete residual stress fields. Fatigue & Fracture of Engineering Materials & Structures 29: 537-545. https://doi.org/10.1111/j.1460-2695.2006.01023.x

Terada H (2011) Stress intensity factor analysis and fatigue behavior of a crack in the residual stress field of welding. Fatigue of Aircraft Structures 1: 5-15. https://doi.org/110.2478/v10164-010-0032-8

Wang K, Huang X, Li Y (2021) Test and prediction of fatigue crack growth rate of titanium alloy materials. Ship Science and Technology 43(3): 13-18. https://doi.org/10.3404/j.issn.1672-7649.2021.03.003 (in Chinese)

Wang Y, Cui W, Wu X, Wang F, Huang X (2008) The extended McEvily model for fatigue crack growth analysis of metal structures. International Journal of Fatigue 30: 1851-1860. https://doi.org/10.1016/j.ijfatigue.2008.01.014

Wu. L (2022) Fatigue crack growth of TC4ELI titanium alloy based on three-dimensional theory. Journal of Ship Mechanics 26(09): 1354-1362. https://doi.org/10.3969/j. issn.1007-7294.2022.09.010 (in Chinese)

Xie X, Jiang W, Luo Y, Xu S, Gong J, Tu S (2017) A model to predict the relaxation of weld residual stress by cyclic load: Experimental and finite element modeling. International Journal of Fatigue 95: 293-301. https://doi.org/10.1016/j.ijfatigue.2016.11.011

Xu X (2013) Effect of residual stress on surface crack growth of welded joints. Dalina: Dalian University of Technology (in Chinese)

Yan G, Crivoi A, Sun Y, Maharjan N, Song X, Li F, Tan M (2018) An Arrhenius equation-based model to predict the residual stress relief of post weld heat treatment of Ti-6Al-4V plate. Journal of Manufacturing Processes 32: 763-772. https://doi.org/10.1016/j.jmapro.2018.04.004

Yi H, Lee Y (2017) Numerical analysis of welding residual stress relaxation in high-strength multilayer weldment under fatigue loads. Metallurgical And Materials Transactions B 48(4): 2164-2175. https://doi.org/10.1007/s11663-017-0958-0

Yu C, Guo Q, Gong X, Yang Y, Zhang J (2022) Fatigue life assessment of pressure hull of deep-sea submergence vehicle. Ocean Engineering 245: 110528. https://doi. org/10.1016/j. oceaneng. 2022.110528

Zaroog O, Ali A, Sahari B, Zahari R (2011) Modeling of residual stress relaxation of fatigue in 2024-T351 aluminium alloy. International Journal of Fatigue 33(2): 279-285. https://doi.org/10.1016/j.ijfatigue.2010.08.012

Zhang W, Jiang W, Zhao X (2018) Fatigue life of a dissimilar welded joint considering the weld residual stress: Experimental and finite element simulation. International Journal of Fatigue 109: 182-190. https://doi.org/10.1016/j.ijfatigue.2018.01.002